Distributed Direct Power Sliding-Mode Control for Islanded AC Microgrids

Carlos Alfaro, Ramon Guzman, *Member IEEE*, Luis Garcia de Vicuña, Hasan Komurcugil, *Senior Member IEEE*, Helena Mart´ın

***Abstract* —The aim of this paper is to develop a novel distributed direct power sliding-mode control for an islanded AC microgrid. This solution replaces the droop mechanism of each inverter with two separate sliding surfaces working as primary/secondary controllers. The design of these surfaces is based on the dynamic model of the active and reactive powers to enhance the robustness against line impedance mismatches. Moreover, a theoretical stability analysis is presented. The main features of this proposed control are: first, regulate the voltage and frequency achieving an accurate active and reactive power sharing; second, achieve stability under a wide range of line impedances; and third provide robustness toward external disturbances, including communication failures. Finally, the experimental results verify the controller performance, the stability with different line impedances, and the robustness against communication partitions.**

***Index Terms*—AC microgrid, distributed control, Sliding-mode control, voltage and frequency regulation.**

I. INTRODUCTION

MICROGRIDS are small power systems that integrate sources, loads, and storages devices using fast acting power inverters. They are attracting more and more interest due to their capability of integrating different kinds of energy resources, as well as global and local loads. They can operate both connected to the main grid or in islanded mode [1], [2].In islanded AC microgrid, a three-layer hierarchical control structure is widely used [3]–[8].

In microgrid control, there exist three main control architectures which are referred to as decentralized, centralized, and distributed. The decentralized control strategies are the most widely accepted due to their reliability and simplicity [9]–[11]. In these approaches, each inverter uses local measurement to implement active and reactive power sharing control. Although the controller does not require communication, these approaches suffer from load dependent frequency/voltage deviations [12]. Moreover, there are some limitations for power sharing in decentralized controllers since it depends on the line impedance [8]. These problems are usually compensated by additional controllers that require communications. In centralized approaches, the active and reactive power sharing control is usually implemented by the conventional droop method [9]. Further, a secondary control is implemented in a central master that calculates the corrective term to eliminate the steady-state voltage and frequency deviation, and then it is sent to the slaves [13]. These approaches require high bandwidth communication among the sources. The main drawback of this approach is that it represents a single point of failure and then replicas are required to improve reliability. Finally, in distributed approaches, each source uses a sparse communication network for data exchange among inverters. The units use only the neighborhood data and calculate its controller using both local measures and data from neighborhood units [14]–[25]. The main advantage of distributed control is the increasing system reliability, decreasing its sensitivity to failure.

Furthermore, many of these control methods are usually synthesized using small-signal equations or suffer from incomplete plant dynamics by using static equations for the active and reactive powers [26]–[28]. Besides, they assume purely inductive or resistive line impedances. Nevertheless, the microgrid impedance may change across time when the sources, loads, and storage devices are connected or disconnected. The mismatch of the line impedance results in inaccurate power sharing and decrease stability [29]. To address the above-mentioned drawback, the droop method may be implemented with a virtual impedance in lines with a high resistance/inductance (R/X) ratio [30]. However, selecting a large value of virtual impedance, the microgrid sensitivity to the feeding loads drastically increases. Moreover, the distortion in the output voltages also increase with unbalanced or nonlinear loads using a virtual impedance.

Recently, distributed controllers attracted more attention in microgrid applications as a promising approach [21]–[25]. In [21], a consensus-based frequency control is proposed for frequency restoration. Further, a distributed finite-time control approach is used in the voltage restoration. Moreover, in [22], a distributed terminal sliding mode controller for the state regulators is applied to achieve active power sharing and state of charge matching. In [23], a distributed SMC is presented

Manuscript received March 01, 2021; revised May 08, 2021, August 18, 2021 and November 11, 2021; accepted December 7, 2021.

This work was supported by the Ministry of Science, Innovation and Universities of Spain and by the European Regional Development Fund under project RTI2018-100732-B-C22.

Carlos Alfaro, Luis Garcia de Vicuña and Helena Martín are with the Department of Electronic and Electrical Engineering, Technical University of Catalonia, 08800 Vilanova i la Geltru, Spain (e-mail: carlos.arturo.alfaro@upc.edu; vicuna@eel.upc.edu; m.helena.martin@upc.edu).

Ramon Guzman is with the Department of Automatic control, Technical University of Catalonia, 08800 Vilanova i la Geltru, Spain (e-mail: ramon.guzman@upc.edu).

Hasan Komurcugil is with the Computer Engineering Department, Eastern Mediterranean University, 99628 Famagusta, Turkey (e-mail:hasan.komurcugil@emu.edu.tr).

for both, frequency and voltage restoration along with accurate active power sharing in islanded microgrid. Besides, in [24], an extended-state-observer secondary voltage and frequency control using an adaptive super twisting algorithm is proposed. This approach is robust against models uncertainties and measurement noise. However, these controllers do not take into account the reactive power sharing. Furthermore, in [25], a distributed primery/secondary droop-inspired control is presented. In this approach, a distributed voltage variance observer is proposed which uses two separate regulator to achieve active and reactive power sharing, respectively. In spite of achieving power sharing and restoring the frequency/voltage deviation, these controllers assume purely inductive lines and are built on top of the artificially imposed separation of concerns that control each type of power, active and reactive, separately. Moreover, in [31] and [32], it has been shown that the system may become unstable in the presence of communication partition for different distributed control approaches.

In this paper, a novel primery/secondary distributed SMC for an islanded AC microgrid is proposed. Unlike the control methods presented above, the model-based control presented in this paper is obtained from a dynamic model based on active and reactive power dynamics equations. The proposed solution is theoretically analyzed for a wide range of line impedances. Moreover, the use of the SMC technique improves the dynamics performance, providing a fast transient response, and robustness against external disturbance and system parameters uncertainties [33]. Finally, the features of the proposed control are the following:

1) High resilience to line impedance values, since the model-based control takes into account that the active and reactive power are coupled.
2) High robustness against system parameters deviations and external perturbations.
3) Sinusoidal three-phase voltages are obtained even in case of feeding unbalanced loads.
4) It achieves accurate active and reactive power sharing.
5) The secondary control is eliminated since frequency and voltage restoration are not necessary.
6) Only a low bandwidth communication network is necessary, thus reducing the traffic of control data.
7) Robustness against communication failures, (e.g. communication partition). This is in direct contrast with the performance of other distributed control approaches that become unstable in case of communication failures [31], [32].

This paper is organized as follows. In section II, the large-signal model of the microgrid is presented. Section III shows the proposed distributed SMC. A stability analysis is presented in section IV. Experimental results are shown in section V. Finally, section VI draws some conclusions of this proposal.

II. Modeling of a Voltage Source Inverter Connected to an AC Microgrid

Fig. 1 illustrates the equivalent circuit of an inverter-based AC microgrid. Focusing on the local behavior of the i^{th} three-phase voltage source inverter (VSI), the VSI$_i$ output voltage

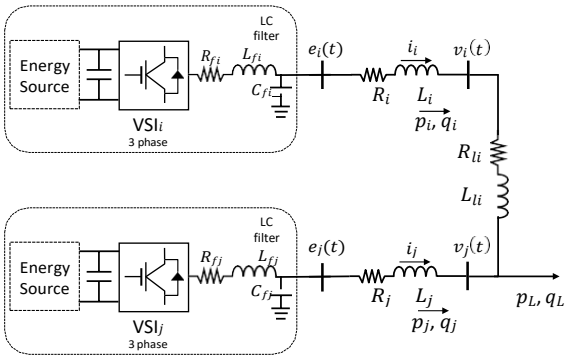

Fig. 1. Schematic diagram of an inverter-based AC microgrid.

can be defined as $e_i(t) = E_i \angle w_o t + \varphi_i$ and the voltage at the connection bus is defined by $v_i(t) = V_i \angle w_o t$. In this figure, E_i and V_i are the amplitude of the VSI$_i$ output voltage and bus voltage, respectively, w_o is the microgrid frequency, φ_i is the phase angle of the VSI$_i$ output voltage, R_i and L_i are the output impedance components, i_i is the VSI$_i$ output current, and p_i and q_i are the instantaneous active and reactive power delivered by the VSI$_i$, respectively.

In the $\alpha\beta$ frame, the equations of the i^{th} instantaneous active and reactive powers can be expressed as follows:

$$p_i = \frac{3}{2}\left(v_{i,\alpha} i_{i,\alpha} + v_{i,\beta} i_{i,\beta}\right) \quad (1)$$

$$q_i = \frac{3}{2}\left(v_{i,\beta} i_{i,\alpha} - v_{i,\alpha} i_{i,\beta}\right) \quad (2)$$

Then, from Fig.1, the differential equations for the i^{th} output current i_i are:

$$\frac{di_{i,\alpha}}{dt} = \frac{1}{L_i}\left(e_{i,\alpha} - i_{i,\alpha} R_i - v_{i,\alpha}\right) \quad (3)$$

$$\frac{di_{i,\beta}}{dt} = \frac{1}{L_i}\left(e_{i,\beta} - i_{i,\beta} R_i - v_{i,\beta}\right) \quad (4)$$

It should be noted from Fig. 1 that, the VSIs dynamics are coupled with each other due to the interconnecting line impedances, R_{li} and L_{li}. These coupling effects are implicit in the bus voltage $v_i(t)$ and can be assumed to be known and bounded below the allowed tolerance [34]. These quantities can be obtained by measurements or estimated from (3) and (4).

The dynamic equations of the instantaneous active and reactive powers can be obtained by taking the first time derivative of (1)-(2), yielding:

$$\frac{dp_i}{dt} = \frac{3}{2}\left(v_{i,\alpha}\frac{di_{i,\alpha}}{dt} + i_{i,\alpha}\frac{dv_{i,\alpha}}{dt} + v_{i,\beta}\frac{di_{i,\beta}}{dt} + i_{i,\beta}\frac{dv_{i,\beta}}{dt}\right) \quad (5)$$

$$\frac{dq_i}{dt} = \frac{3}{2}\left(v_{i,\beta}\frac{di_{i,\alpha}}{dt} + i_{i,\alpha}\frac{dv_{i,\beta}}{dt} - v_{i,\alpha}\frac{di_{i,\beta}}{dt} - i_{i,\beta}\frac{dv_{i,\alpha}}{dt}\right) \quad (6)$$

Then, using the definition of $e_i(t)$ and $v_{b,i}(t)$ and (3) - (4) in (5) and (6), the dynamic equations of the active and reactive powers delivered by the VSI$_i$ to the microgrid can be rewritten

as follows:

$$\frac{dp_i}{dt} = \frac{3}{2L_i}\left(-V_i^2 + E_i V_i \cos(\varphi_i - \varphi_i)\right) - \frac{R_i}{L_i} p_i + D_p \quad (7)$$

$$\frac{dq_i}{dt} = -\frac{3}{2L_i} E_i V_i \sin(\varphi_i) - \frac{R_i}{L_i} q_i + D_q \quad (8)$$

where D_p and D_q are the inverters coupled dynamic terms represented as known disturbances in this model. These disturbances include the unbalanced voltages and nonlinear loads presented in the microgrid and are expressed as:

$$D_p(t) = \frac{3}{2}\left(i_{i,\alpha}\frac{dv_{i,\alpha}}{dt} + i_{i,\beta}\frac{dv_{i,\beta}}{dt}\right) \quad (9)$$

$$D_q(t) = \frac{3}{2}\left(i_{i,\alpha}\frac{dv_{i,\beta}}{dt} - i_{i,\beta}\frac{dv_{i,\alpha}}{dt}\right) \quad (10)$$

Besides, taking the first derivative of p_i and q_i equal to zero, the steady-state expressions of the active and reactive powers can be written as:

$$P_i = \frac{3V_i}{2Z_i}\left[(E\cos(\varphi_i - \varphi_i) - V_i)\cos(\phi_i) + E_i \sin(\phi_i)\sin(\varphi_i - \varphi_i)\right] \quad (11)$$

$$Q_i = \frac{3V_i}{2Z_i}\left[(E\cos(\varphi_i) - V_i)\sin(\phi_i) - E_i\cos(\phi_i)\sin(\varphi_i)\right] \quad (12)$$

Note that, in previous works, the control architecture is based on steady-state expressions P_i and Q_i [9]–[16].

In this paper, unlike existing works, the controller is derived using the dynamic equations (7) and (8). However, it is considered that the phase angle φ_i is relatively small in practice, then the approximations $\cos(\varphi_i) \approx 1$ and $\sin(\varphi_i) \approx \varphi_i$ can be used. Finally, taking into account the above assumptions, (7) and (8) can be rewritten as:

$$\frac{dp_i}{dt} = \frac{3}{2L_i}\left(-V_i^2 + E_i V_i - \frac{R_i}{L_i} p_i + D_p\right) \quad (13)$$

$$\frac{dq_i}{dt} = -\frac{3}{2L_i} E_i V_i \varphi_i - \frac{R_i}{L_i} q_i + D_q \quad (14)$$

Note that, the presented microgrid model is a multi-input multi-output (MIMO) nonlinear system.

III. Proposed Control System

A. Control objectives

The main objective of a VSI connected to an islanded microgrid is to regulate the frequency and amplitude of the microgrid voltage. Furthermore, with the aim to avoid the overstressing and deteriorating of the source, it is required to share the total load demand among the sources (i.e. active and reactive power sharing). Taking this in mind, the objectives of the proposed controller are the following:

1) The voltage amplitude is a local variable in a microgrid with different values for each inverter in steady-state. Thus, the first objective is to regulate the voltage amplitude so that the average amplitude considering the other inverters coincides with the nominal value.
2) The frequency is a global variable in a microgrid with the same value for each inverter in steady state. Thus, the second objective is that the steady-state frequency of each inverter matches the nominal frequency.
3) The third objective is to guarantee active and reactive power sharing

In order to achieve the above objectives, in this paper a novel distributed SMC for VSIs connected to a microgrid is proposed. Furthermore, to achieve accurate power sharing and to regulate the voltage amplitude, the following error functions are proposed:

$$e_{p,i} = p_i^* - p_i \quad (15)$$

$$e_{q,i} = q_i^* - q_i \quad (16)$$

$$e_{E,i} = E_o^* - E_{a,i} \quad (17)$$

where p_i^* and q_i^* are the active and reactive power references, respectively, E_o^* is the voltage amplitude reference and $E_{a,i}$ is the average microgrid voltage. To calculate the power references and the average microgrid voltage, the proposal uses communication between the n_i neighborhood VSIs. Thus, the references are calculated as follows:

$$p_i^* = p_i^{max}\sum_{j=1}^{n_i}\frac{a_{ij}p_j^{rated}}{n_i} \quad (18)$$

$$q_i^* = q_i^{max}\sum_{j=1}^{n_i}\frac{a_{ij}q_j^{rated}}{n_i} \quad (19)$$

$$E_{a,i} = \sum_{j=1}^{n_i}\frac{a_{ij}E_j}{n_i} \quad (20)$$

where p_i^{max} and q_i^{max} are the maximum active and reactive power supplied by source i, and p_j^{rated} and q_j^{rated} are expressed as:

$$p_j^{rated} = \frac{p_j}{p_j^{max}} \quad (21)$$

$$q_j^{rated} = \frac{q_j}{q_j^{max}} \quad (22)$$

Finally, the communication system model is a connected graph with a spanning tree, where the coefficients a_{ij} determine the availability of communication between inverters i and j, thus indicating the set of nodes n_i that exchange control data. Hence, $a_{ij} = a_{ji} = 1$ if nodes i and j can exchange their information and $a_{ij} = a_{ji} = 0$ otherwise.

B. Proposed sliding mode control

In order to reach the control objectives presented above, the voltage amplitude and phase angle are expressed as:

$$\varphi_i = u_{\varphi_i} \quad (23)$$

$$E_i = V_o + u_{E_i} \quad (24)$$

where V_o is microgrid nominal voltage. Moreover, in order to avoid the chattering problems, and allow continuous control actions, a high-order sliding mode controller is proposed [35], [36]. Therefore, the first time derivative of u_{φ_i} and u_{E_i} are expressed as follows:

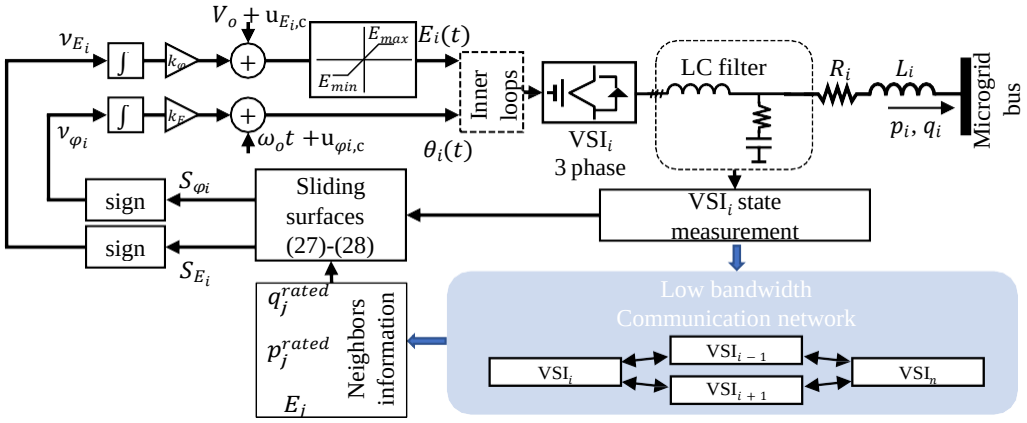

Fig. 2. Diagram of the proposed control scheme

$$\frac{du_{\varphi_i}}{dt} = k_\varphi v_{\varphi_i} + v_{\varphi_i,eq} \tag{25}$$

$$\frac{du_{E_i}}{dt} = k_E v_{E_i} + v_{E_i eq} \tag{26}$$

where v_{E_i} and v_{φ_i} are the switching control variables, and $v_{E_i,eq}$ and $v_{\varphi_i,eq}$ are the equivalent controls.

Then, the proposed sliding surfaces are expressed as:

$$S_{E,i} = -\frac{dp_i}{dt} + k_p e_{p,i} + k_{\delta E} e_{e,i} \tag{27}$$

$$S_{\varphi,i} = \frac{dq_i}{dt} - k_q e_{q,i} \tag{28}$$

where k_p, k_q and $k_{\delta E}$ are positive definite. In the sliding mode regime, the sliding surfaces $S_{\varphi,i} = 0$ represent the precise tracking of reactive power with a first order dynamic behavior. On the other hand, when $S_{E,i} = 0$, the voltage amplitude and the active power dynamic in sliding mode regime is quite similar to a resistive droop controller with a proportional secondary control [4]. Moreover, in steady-state the controller is allowed to regulate the average voltage amplitude and the active power sharing.

C. Control law

In the sliding mode controller, the control law usually consists of the equivalent control and the switching control. The equivalent control keeps the state of the system on the sliding surface, while the switching control forces the system sliding on the sliding surface.

First, in order to satisfy reaching conditions of sliding mode controllers $S_{E,i}\dot{S}_{E,i} < 0$ and $S_{\varphi,i}\dot{S}_{\varphi,i} < 0$, we must choose the switching controls whose control laws are expressed as follows:

$$v_{E,i} = \begin{cases} 1 & if \quad S_{E,i} > 0 \\ -1 & if \quad S_{E,i} < 0 \end{cases} \tag{29}$$

$$v_{\varphi,i} = \begin{cases} 1 & if \quad S_{\varphi,i} > 0 \\ -1 & if \quad S_{\varphi,i} < 0 \end{cases} \tag{30}$$

Second, assuming that the system is in the sliding mode regime, and taking into account that in sliding regime it is accomplished that $\dot{S} = S = 0$. The integral of the equivalent controls $v_{E_i,eq}(t)$ and $v_{\varphi_i,eq}(t)$ can be obtained by taking the sliding surfaces equal to zero. Thus, considering the microgrid model (13) and (14), the voltage amplitude and angle definitions (25) and (26), and the sliding surfaces (27) and (28), the following expressions can be obtained:

$$\int_0^t v_{\varphi_i,eq}\, dt = \frac{2L_i}{3V_i E_i}\left(\frac{R_i}{L_i} q_i + D_q - \frac{2L_i}{3V_i E_i}(k_q e_{q,i})\right) \tag{31}$$

$$\int_0^t v_{E_i,eq} dt = (V_i - V_o) + \frac{2L_i}{3V_i}\left(\frac{R_i}{L_i} p_i - D_p + \frac{2L_i}{3V_i}(k_p e_{p,i} + k_{\delta E} e_{e,i})\right) \tag{32}$$

where R_i and L_i are the local inverter impedances (see Fig. 1). Furthermore, it is worth noting that the disturbances modeling in (9) and (10) are used as feedforward terms, thus bringing robustness against the coupled inverters dynamics and microgrid perturbation, such as unbalanced and nonlinear loads.

Finally, according to the control laws (29) and (30), and (31) and (32), the voltage amplitude and phase angle set points, (23) and (24), respectively, can be rewritten as follows:

$$\varphi_i = k_\varphi \int_0^t sign(S_{\varphi,i}) dt + \int_0^t v_{\varphi_i,eq} dt \tag{33}$$

$$E_i = V_o + k_E \int_0^t sign(S_{E,i}) dt + \int_0^t v_{E_i,eq} dt \tag{34}$$

where k_φ and k_E are the control gains.

It should be noted that the discontinuous sign functions only appear in the time derivatives of the actual control inputs, thus allowing continuous control actions. Besides, the control law does not depend on the line impedances, hence the virtual impedances are not needed.

D. Stability analysis

The stability analysis is carried out using the Lyapunov criteria. Let V_e and V_φ be the Lyapunov function candidates,

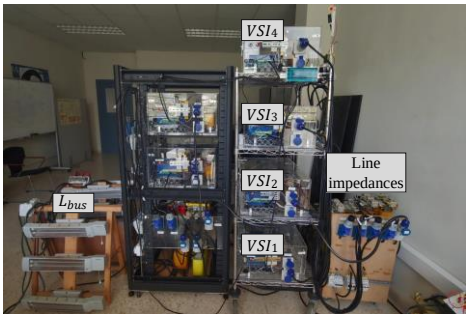

Fig. 3. Photograph of the experimental microgrid.

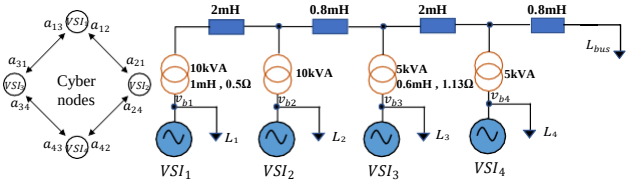

Fig. 4. Diagram of the laboratory microgrid setup.

such that

$$V_e = \frac{1}{2} S_{E,i}^2 \tag{35}$$

$$V_\varphi = \frac{1}{2} S_{\varphi,i}^2 \tag{36}$$

the time derivative of (35) and (36) can be expressed as follows:

$$\dot{V}_e = S_{E,i} \dot{S}_{E,i} \tag{37}$$

$$\dot{V}_\varphi = S_{\varphi,i} \dot{S}_{\varphi,i} \tag{38}$$

Then, in order to prove the stability, it is sufficient to achieve the following conditions $\dot{V}_e < 0$ and $\dot{V}_\varphi < 0$. Therefore, the stability is achieved if the above conditions are satisfied. Taking this in mind, from (25), (26), (31), (32), (33) and (34), and using (27) and (28), the above equations can be rewritten as follows:

$$\dot{V}_e = S_{E,i}(-k_E sign(S_{E,i})) \tag{39}$$

$$\dot{V}_\varphi = S_{\varphi,i}(-k_\varphi sign(S_{\varphi,i})) \tag{40}$$

From (39) and (40), it can be noted that the time derivative of Lyapunov function is definitely negative, hence the control system becomes asymptotically stable. Additionally, it should be noted that even under the absence of communication network the stability condition is still achieved.

E. Controller implementation

In this section the proposed controller implementation is presented.

Fig. 2 shows the proposed control scheme for the i^{th} VSI. The proposal is based on two sliding surfaces to generate the output voltage references of each VSI. As can be seen in (27), (28), (31) and (32), the control laws (33) and (34) use local and neighborhood data. In order to achieve the control objectives, the communication system model is a connected graph with a spanning tree, where the neighborhood inverters exchange their voltage amplitude, active and reactive rated power, and thus the errors are calculated. For this purpose, the control system uses a low bandwidth communication network to interchange data between the neighborhood sources. Additionally, when the communications fail, the proposed controller could work with the local data remaining the system stability, such as the droop control, however, the steady-state could be compromised [37].

Then, once the local and neighborhood data is obtained, the sliding surfaces and the control variables $u_{\varphi_i,d}$, $u_{E_i,d}$, $u_{\varphi_i,c}$ and $u_{E_i,c}$ are calculated to obtain the voltage amplitude and angle phase set points using (23) and (24). Moreover, in order to maintain the allowed tolerance [34], E_i is bounded between ±5% of the nominal value, as it can be seen in Fig. 2. Finally, once the voltage set point is computed, the inner loop is responsible to generate the voltage signals. Therefore, voltage set point used by the inner loop is expressed as follows:

$$e_i^* = E_i sin(\vartheta_i) \tag{41}$$

$$\vartheta_i = \omega_o t + \varphi_i. \tag{42}$$

TABLE I
OUTPUT IMPEDANCES

Description	Symbol	Value
VSI 1 output impedance	Z_1	$0.5 + 2.64j\ \Omega$
VSI 2 output impedance	Z_2	$0.5 + 2.64j\ \Omega$
VSI 3 output impedance	Z_3	$0.5 + 1.88j\ \Omega$
VSI 4 output impedance	Z_4	$0.5 + 1.88j\ \Omega$

TABLE II
EQUIVALENT LINE IMPEDANCE

Description	Value	(X/R) ratio
Impedances seen by VSI 1	$0.76 + 1.34j\ \Omega$	1.76
Impedances seen by VSI 2	$0.80 + 0.74j\ \Omega$	0.92
Impedances seen by VSI 3	$1.32 + 0.87j\ \Omega$	0.30
Impedances seen by VSI 4	$1.30 + 0.76j\ \Omega$	0.59

IV. Experimental Results

A. Microgrid Setup

This section presents the experimental tests implemented in the laboratory microgrid shown in Fig. 3 and 4. Fig. 4 illustrates the diagram of the laboratory inverter-based islanded microgrid considered in this study. This is formed by four inverters working as VSIs, each one with local loads that may be connected or disconnected. Moreover, two three-phase balanced loads are considered to be connected to the microgrid each that may be connected or disconnected in the position shown in Fig. 4 to form the global load L_{bus}.

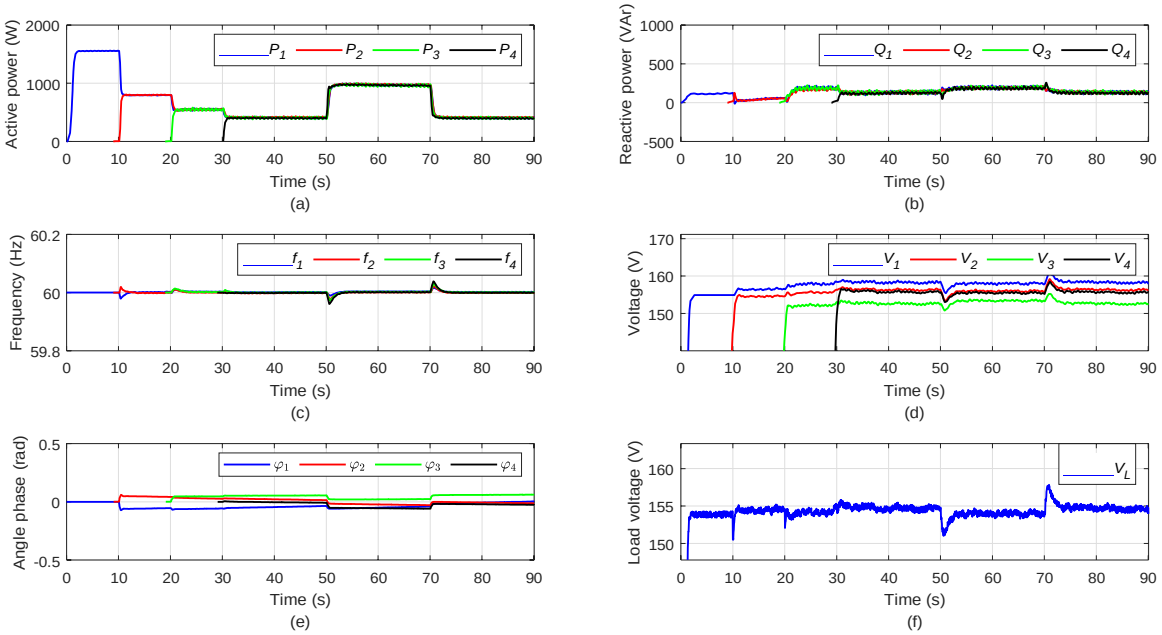

Fig. 5. Performance evaluation of the proposed controller: (a) inverter active power, (b) inverter reactive power, (c) inverter frequencies, (d) bus voltage, (e) phase angles and (f) load voltage.

Moreover, from Table I the output impedance of each inverter is presented. In Table II, it should be noted that the inverter 1 line impedance is mainly inductive while the inverter 3, and 4 line impedances are mainly resistive. In addition, the inverter 2 line impedance presents no dominant behavior. Taking all these impedances in mind, it is clear that the microgrid is operating in a mixed scenario with resistive, inductive and complex impedances. Each inverter was built using a 2.3-kVA Guasch MTL-CBI0060F12IXHF full bridge as the power converter and is driven by a 32-bit dual-core DSP, the Concerto-F28M36P63C with a sampling frequency of 10 kHz. This device is composed of a C28 DSP core for control purposes and a Cortex M3 ARM for communication. The communication between each VSI is based on the UDP Protocol over an Ethernet link that communicates the four C28 cores through the M3 cores with a transmission time of 0.1 s. The communication configuration is represented by the cyber nodes shown in Fig. 4. The bidirectional arrows represent the availability of communication between inverters. Finally, the control gains k_φ and k_E have been selected as k_φ = 0.1 and k_E = 1 as can be seen in table III.

TABLE III
SYSTEM PARAMETERS

Description	Symbol	Value
Microgrid voltage	V_o	110 V_{rms}
Microgrid frequency	f	60 Hz
Nominal dc-link voltage	V_{dc}	400 V
Active power gain	k_p	250
Reactive power gain	k_q	250
Voltage amplitude gain	$k_{\delta E}$	1000
Voltage control gain	k_E	1
Phase angle control gains	k_φ	0.1
Maximum active power 1-4	$P^{max}_{1,2,3,4}$	2000 W
Maximum reactive power 1-4	$Q^{max}_{1,2,3,4}$	2000 VAr
Sampling frequency	f_s	10 kHz

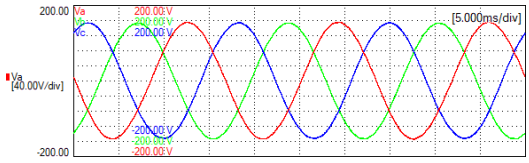

Fig. 6. Load voltages using the proposed control scheme.

B. Performance evaluation in Normal Operation

To validate the performance of the proposed distributed SMC with the parameters shows in Table III, the following experimental test was designed in the laboratory setup. First, to validate the plug and play capability, the four VSIs are connected at different time, t =0, 10, 20 and 30 s respectively. The first inverter starts and fixes the microgrid frequency and voltage, to their rated values, while starting to feed a balanced load connected in the bus, with a total power demand above 1.6 kW. The activation of the following inverters is done using a phase-locked loop for synchronizing them to the microgrid voltage phase. Then, to validate the performance of the microgrid under sudden load change, the second three-phase balanced load is connected and disconnected at t =50 and 70 s respectively.

Fig. 5 shows the active and reactive power by each inverter, as well as their frequencies, voltage amplitudes, the phase angles φ_i and the amplitude correction terms δE_i. Fig. 5 (a) and Fig. 5 (b) show active and reactive powers, as it can

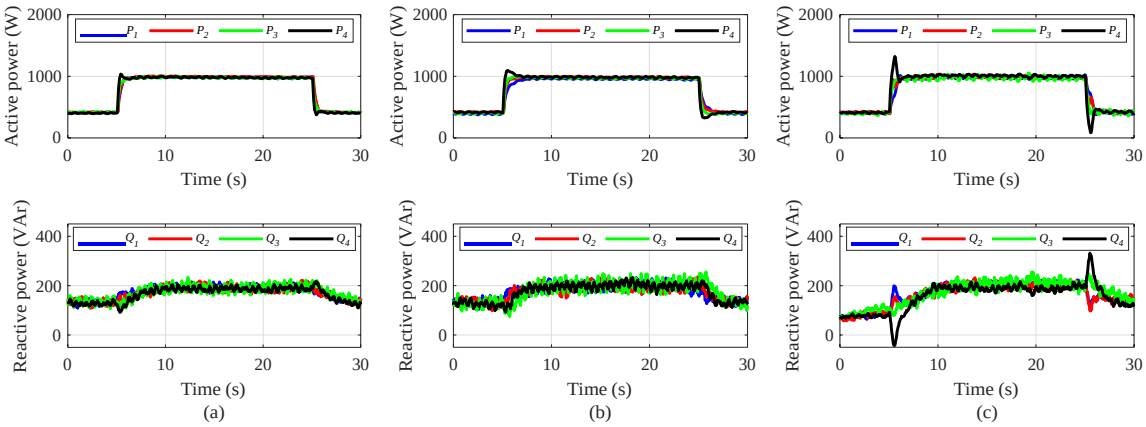

Fig. 7. Active and reactive power transient responses with different transmission rates: (a) 0.1 s, (b) 0.5 s and (c) 1 s.

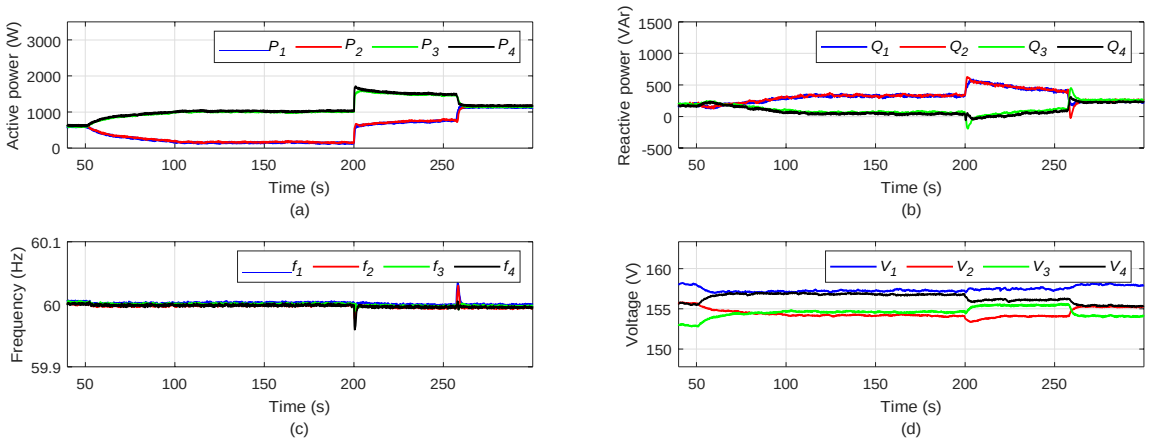

Fig. 8. System dynamics when a communication failure leads to two partitions: (a) inverter active power, (b) inverter reactive power, (c) inverter frequencies, and (d) bus voltage.

be seen after each connection the active and reactive power sharing is achieved with a good dynamic response. Moreover, Fig. 5 (c) shows that all inverter frequencies are synchronized to the rated frequency of 60 Hz in steady state. Further, Fig. 5 (e) shows that the phase angles are small and smooth. Moreover, Fig. 5 (d) show two interesting points. First, the amplitude of the output voltages are different in each inverter. And second, the average value of these voltage amplitudes in steady-state is perfectly regulated to the nominal value V_o. Finally, Fig. 5 (f) shows the amplitude of the load voltage, and it can be seen that the voltage is regulated with a tolerance less than 5% of its nominal value. These characteristics are maintained during the whole experiment with different loads and number of inverters in operation. Thus, it is demonstrated that the proposed controller achieves the control objectives presented in section III. Additionally, Fig. 6 shows the voltage waveforms of the load bus. It can be noted that the voltage waveforms are balanced with sinusoidal form.

C. Communication Failure Study

The distributed control system relies on the availability of communications. Besides, in large distributed systems the units may be far away, thus the communication services may be affected, such as transmission delay, communication link failures, etc. Accordingly, communication failures may compromise the overall control performance and the system may be driven to instability. Moreover, recent studies have shown that for different distributed control approaches the microgrid may become unstable when a communication partition is presented [31], [32]. Thus, to show the performance of the proposed control in the presence of communication failures, two different tests were designed.

In the first experiment, the proposed control has been tested under a sudden load change with different transmission rates. Fig. 7 shows the active power and reactive power of the four VSIs under different transmission rates. Fig. 7(a) shows the active and reactive power performance with the nominal transmission rate of 0.1. Besides, in Fig. 7(b) and (c) the active and reactive power transient responses are shown with a transmission rate of 0.5 and 1 s, respectively. From Fig. 7 it should be noted that the steady-state is not compromised by the transmission delay. However, the transient response of both active and reactive power is slightly deteriorated when the transmission rate increases.

In the second experiment, the proposed control has been tested in presence of communication links failure. For this purpose the following experiment was designed. At the time t =0

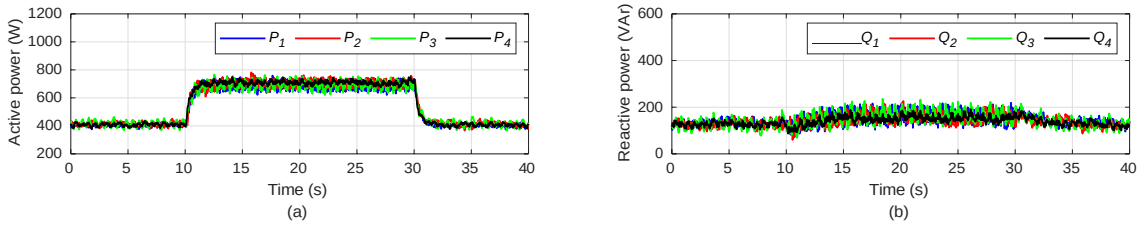

Fig. 9. System dynamics feeding an unbalanced load: (a) inverter active power and (b) inverter reactive power.

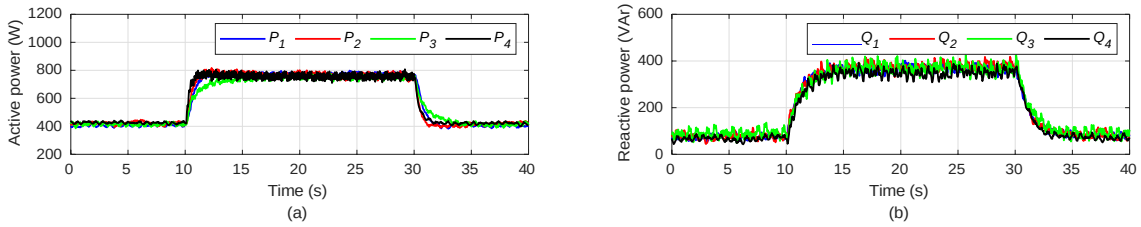

Fig. 10. System dynamics feeding nonlinear load: (a) inverter active power and (b) inverter reactive power.

s, the four VSIs are previously working in normal condition feeding a three-phase balanced load. Then, at time t =50 s the communication links 1-3 and 2-4 have been disabled during 250 s, and at time t = 300 s, communications are reestablished. Besides, the second three-phase balanced load is connected at t =200 s. Hence, the system emulates a partition in the communication network. Fig. 8 shows the active and reactive power, as well as the frequencies and voltage amplitude of each VSI when the communication partition occurs. It should be noted that after the partition occurs, all inverter frequencies are synchronized to the rated frequency of 60 Hz and the average voltage amplitude is regulated to the nominal value V_o. However, the active and reactive power sharing between the two communication islands is not achieved. It is because the distributed control starts working as "two" parallel controls independent among them. Despite this, the proposed control avoids the instability problem. This is a superior feature of the proposed control in comparison with others [31], [32]

D. Three-Phase Unbalanced Load Study

In the third experiment, the proposed controller has been tested under a three-phase unbalanced load. For this purpose, the following experiment has been designed. The four VSIs start feeding a three-phase balanced load, then an unbalanced load is connected and disconnected in L_{bus} at time t =20 and 40 s, respectively. Fig. 9 shows the active and reactive power of each VSI. Moreover, Fig. 11 shows the current and voltage waveforms of inverter 1. In Fig. 9, it can be seen that after the unbalanced load is connected, the active and reactive power sharing is achieved. As a promising characteristic, note that the proposed control does not need a virtual impendence due to its robustness against line impedance uncertainties, as it was demonstrated in section IV. Accordingly, the VSIs voltage waveforms are balanced even with unbalanced current waveforms, as it has been shown in Fig. 11.

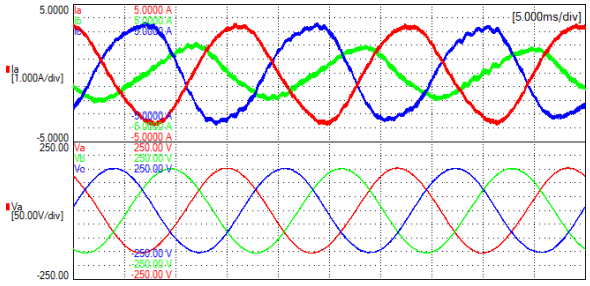

Fig. 11. Inverter 1 current and voltage using the proposed control scheme under unbalanced load.

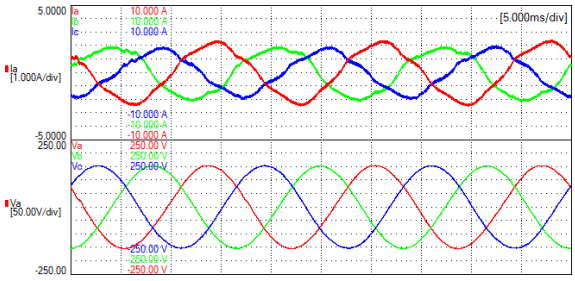

Fig. 12. Inverter 1 current and voltage using the proposed control scheme feeding a nonlinear load.

E. Nonlinear Load Study

Finally, the proposed controller has been tested under a non-linear load (three phase diode rectifier). Taking this in mind, the following experiment has been designed. The four VSIs start feeding a three-phase balanced load, then a nonlinear load is connected and disconnected in L_{bus} at time t =20 and 40 s, respectively. Fig. 10 shows the active and reactive power. Besides, Fig. 12 shows the current and voltage waveforms of inverter 1, respectively. From Fig. 10, it should be noted that the active and reactive power sharing is achieved even feeding a nonlinear load. Finally, in Fig 12 it should be noted that the current waveforms are distorted with a THD of 15.1%.

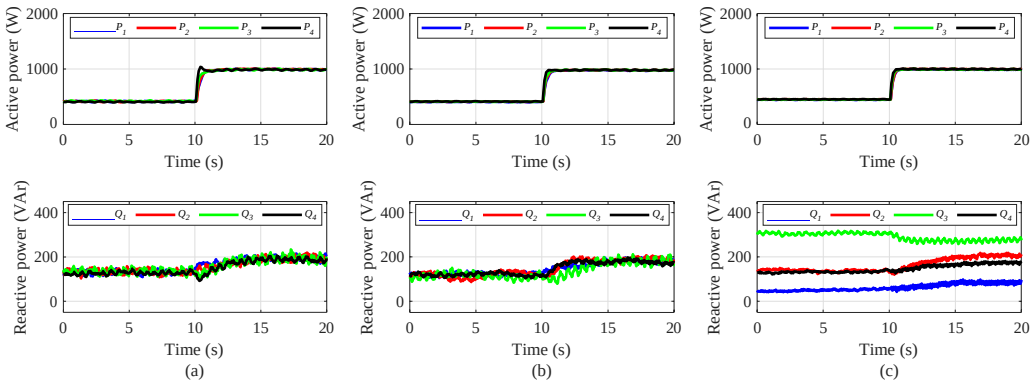

Fig. 13. Active and reactive power transient response comparison of different control schemes: (a) proposed controller, (b) Droop-free control [25] and (c) Distributed robust secondary control [24].

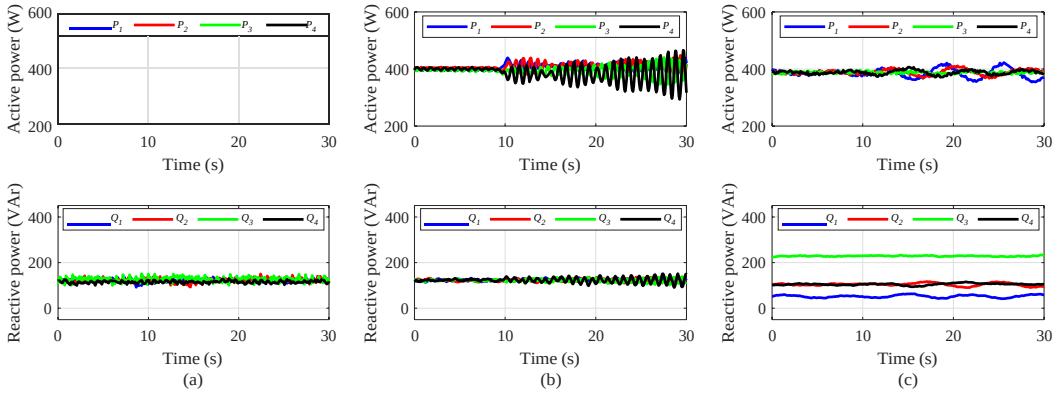

Fig. 14. Active and reactive power steady state behavior without virtual impedance: (a) proposed controller, (b) Droop-free control [25] and (c) Distributed robust secondary control [24].

Meanwhile, the voltage waveforms have a sinusoidal form when the nonlinear load is connected with a THD of 1.5% approximately.

F. Comparison with State-of-the-art Techniques

This subsection presents a comparison between the proposed control and previous state-of-the-art controllers. For this purpose,the proposal will be compared with the droop-free controller [25] and a distributed robust secondary control [24]. It is worth noting that the control parameters of each policy have been defined to obtain similar dynamics among them. Moreover, to yield stability and increase the accurate power sharing, the droop-free and the distributed robust secondary control need a virtual impedance [30].

In order to validate the dynamic performance of the proposed control scheme, two experiments have been performed. First, the controllers have been tested under a sudden load change. This experimental test has the following pattern. From t =0 s to t =10 s the inverters start feeding a balanced load connected in L_{bus} , with a total power demand above 1.6 kW. Then, a second balanced load is connected in L_{bus} at time t =10. Fig. 13 shows the experimental results of the considered control schemes under a sudden load change. It should be noted that the active power transient response is similar in the three control schemes. However, from Fig. 13 (c) it can be seen that the reactive power is not shared using the method in [24].

In the second experiment, the controllers [25] and [24] are initially driven with a virtual impedance. Then, at t = 10 s the virtual impedance is removed from the control schemes [25] and [24]. It is worth noting that the proposed controller does not need virtual impedance. Fig. 14 shows the active and reactive power by each inverter using the proposed SMC, [25] and [24]. It could be noted that, when the virtual impedance is removed, both the droop-free controller [25] and the distributed robust secondary control [24] dynamics is oscillatory and unstable. It is due to the power lines mismatches [29], since the microgrid is operating in a mixed scenario with resistive, inductive and complex impedances, as it can be seen in Table II.

Finally, Table IV is presented to compare the proposed controller with the state-of-the-art controllers. The comparison is done in terms of accurate active and reactive power sharing, steady-state voltage and frequency deviation, resilience to line impedance ratio and robustness against communication partitions. According to the experimental results and Table IV, it can be seen that the proposed control is more beneficial in terms of accurate active and reactive power without voltage deviation and robustness against communication failures.

TABLE IV
COMPARATIVE ANALYSIS

Control Method	Power sharing	f and V regulation	Resilience to R/X ratio	Comms. partition
[21]	only p	Yes	No	instable
[22]	only p	Yes	No	Not shown
[23]	only p	Yes	No	Not shown
[24]	only p	Yes	No	Not shown
[25]	p and q	Yes	No	instable
Proposed	p and q	Yes	Yes	stable

V. Conclusions

A novel distributed direct power sliding mode control has been proposed in this paper for AC microgrids. This control relies on the availability of communications. The control is formed by two sliding surfaces based on the microgrid model equations, with the following properties. On the one hand, the controller regulates the average voltage across the microgrid to the nominal value. On the other hand, the controller compares the local active and reactive power with the neighbors, to achieve a zero steady-state error in active and reactive power sharing. Besides, a stability analysis is presented to probe the controller robustness against line impedance uncertainties. Experimental results show that the proposed controller provides voltage regulation and a precise active and reactive power sharing, as well as frequency synchronization to the rated value under various load types, even in case of unbalanced loads. Moreover, the experimental results have also shown that the proposed control presents both plug and play capability and high robustness against communication failures.

References

[1] R. H. Lasseter, "Microgrids and distributed generation," *Journal of Energy Engineering*, vol. 133, no. 3, pp. 144–149, 2007.

[2] R. H. Lasseter, "Certs microgrid," in *2007 IEEE International Conference on System of Systems Engineering*, 2007, pp. 1–5.

[3] J. M. Guerrero, J. C. Vasquez, J. Matas, L. Garc´ıa de Vicuna, and M. Castilla, "Hierarchical control of droop-controlled AC and DC microgrids. A general approach towards standardization," *IEEE Trans. Ind. Electron.*, vol. 58, no. 1, pp. 158–172, Jan. 2011.

[4] A. Bidram and A. Davoudi, "Hierarchical structure of microgrids control system," *IEEE Trans. Smart Grid*, vol. 3, no. 4, pp. 1963–1976, 2012.

[5] T. L. Vandoorn, J. C. Vasquez, J. De Kooning, J. M. Guerrero, and L. Vandevelde, "Microgrids: Hierarchical control and an overview of the control and reserve management strategies," *IEEE Ind. Electron. Mag.*, vol. 7, no. 4, pp. 42–55, 2013.

[6] J. Rocabert, A. Luna, F. Blaabjerg, and P. Rodr´ıguez, "Control of power converters in ac microgrids," *IEEE Trans. Power Electron.*, vol. 27, no. 11, pp. 4734–4749, 2012.

[7] D. E. Olivares, A. Mehrizi-Sani, A. H. Etemadi, C. A. Cañizares, R. Iravani, M. Kazerani, A. H. Hajimiragha, O. Gomis-Bellmunt, M. Saeedifard, R. Palma-Behnke, G. A. Jiménez-Estévez, and N. D. Hatziargyriou, "Trends in microgrid control," *IEEE Trans. Smart Grid*, vol. 5, no. 4, pp. 1905–1919, 2014.

[8] Y. Han, H. Li, P. Shen, E. A. A. Coelho, and J. M. Guerrero, "Review of active and reactive power sharing strategies in hierarchical controlled microgrids," *IEEE Trans. Power Electron.*, vol. 32, no. 3, pp. 2427–2451, 2017.

[9] J. M. Guerrero, J. Matas, L. Garcia De Vicuna, M. Castilla, and J. Miret, "Wireless-control strategy for parallel operation of distributed-generation inverters," *IEEE Trans. Ind. Electron.*, vol. 53, no. 5, pp. 1461–1470, 2006.

[10] R. Majumder, A. Ghosh, G. Ledwich, and F. Zare, "Angle droop versus frequency droop in a voltage source converter based autonomous microgrid," in *2009 IEEE Power Energy Society General Meeting*, 2009, pp. 1–8.

[11] E. Rokrok and M. E. H. Golshan, "Adaptive voltage droop scheme for voltage source converters in an islanded multibus microgrid," *IET Generation, Transmission Distribution*, vol. 4, no. 5, pp. 562–578, 2010.

[12] M. Castilla, A. Camacho, P. Mart´ı, M. Velasco, and M. M. Ghahderijani, "Impact of clock drifts on communication-free secondary control schemes for inverter-based islanded microgrids," *IEEE Trans. Ind. Electron.*, vol. 65, no. 6, pp. 4739–4749, 2018.

[13] A. G. Tsikalakis and N. D. Hatziargyriou, "Centralized control for optimizing microgrids operation," in *2011 IEEE Power and Energy Society General Meeting*, 2011, pp. 1–8.

[14] F. Guo, C. Wen, J. Mao, and Y. Song, "Distributed secondary voltage and frequency restoration control of droop-controlled inverter-based microgrids," *IEEE Trans. Ind. Electron.*, vol. 62, no. 7, pp. 4355–4364, 2015.

[15] A. Bidram, A. Davoudi, and F. L. Lewis, "A multiobjective distributed control framework for islanded ac microgrids," *IEEE Trans. on Industrial Informatics*, vol. 10, no. 3, pp. 1785–1798, 2014.

[16] V. Nasirian, Q. Shafiee, J. M. Guerrero, F. L. Lewis, and A. Davoudi, "Droop-free distributed control for ac microgrids," *IEEE Trans. Power Electron.*, vol. 31, no. 2, pp. 1600–1617, 2016.

[17] Z. Li, Z. Cheng, J. Liang, J. Si, L. Dong, and S. Li, "Distributed event-triggered secondary control for economic dispatch and frequency restoration control of droop-controlled ac microgrids," *IEEE Transactions on Sustainable Energy*, vol. 11, no. 3, pp. 1938–1950, 2020.

[18] Y. Zhang, A. M. Shotorbani, L. Wang, and B. Mohammadi-Ivatloo, "Distributed secondary control of a microgrid with a generalized pi finite-time controller," *IEEE Open Access Journal of Power and Energy*, vol. 8, pp. 57–67, 2021.

[19] N. M. Dehkordi, N. Sadati, and M. Hamzeh, "Distributed robust finite-time secondary voltage and frequency control of islanded microgrids," *IEEE Trans. Power Syst.*, vol. 32, no. 5, pp. 3648–3659, 2017.

[20] A. Pilloni, A. Pisano, and E. Usai, "Robust finite-time frequency and voltage restoration of inverter-based microgrids via sliding-mode cooperative control," *IEEE Trans. Ind. Electron.*, vol. 65, no. 1, pp. 907–917, 2018.

[21] Q. Shafiee, J. M. Guerrero, and J. C. Vasquez, "Distributed secondary control for islanded microgrids—a novel approach," *IEEE Trans. Power Electron.*, vol. 29, no. 2, pp. 1018–1031, 2014.

[22] A. M. Shotorbani, S. Ghassem-Zadeh, B. Mohammadi-Ivatloo, and S. H. Hosseini, "A distributed secondary scheme with terminal sliding mode controller for energy storages in an islanded microgrid," *International Journal of Electrical Power Energy Systems*, vol. 93, pp. 352–364, 2017.

[23] N. Sarrafan, M. A. Rostami, J. Zarei, R. Razavi-Far, M. Saif, and T. Dragicevic, "Improved distributed prescribed finite-time secondary control of inverter-based microgrids: Design and real-time implementation," *IEEE Trans. Ind. Electron.*, pp. 1–1, 2020.

[24] P. Ge, X. Dou, X. Quan, Q. Hu, W. Sheng, Z. Wu, and W. Gu, "Extended-state-observer-based distributed robust secondary voltage and frequency control for an autonomous microgrid," *IEEE Transactions on Sustainable Energy*, vol. 11, no. 1, pp. 195–205, 2020.

[25] S. M. Mohiuddin and J. Qi, "Droop-free distributed control for ac microgrids with precisely regulated voltage variance and admissible voltage profile guarantees," *IEEE Transactions on Smart Grid*, vol. 11, no. 3, pp. 1956–1967, 2020.

[26] E. A. A. Coelho, P. C. Cortizo, and P. F. D. Garcia, "Small signal stability for single phase inverter connected to stiff ac system," in *Conference Record of the 1999 IEEE Industry Applications Conference. Thirty-Forth IAS Annual Meeting*, vol. 4, 1999, pp. 2180–2187 vol.4.

[27] X. Guo, Z. Lu, B. Wang, X. Sun, L. Wang, and J. M. Guerrero, "Dynamic phasors-based modeling and stability analysis of droop-controlled inverters for microgrid applications," *IEEE Trans. Smart Grid*, vol. 5, no. 6, pp. 2980–2987, 2014.

[28] M. Farrokhabadi, C. A. Cañizares, J. W. Simpson-Porco, E. Nasr, L. Fan, P. A. Mendoza-Araya, R. Tonkoski, U. Tamrakar, N. Hatziargyriou, D. Lagos, R. W. Wies, M. Paolone, M. Liserre, L. Meegahapola, M. Kabalan, A. H. Hajimiragha, D. Peralta, M. A. Elizondo, K. P. Schneider, F. K. Tuffner, and J. Reilly, "Microgrid stability definitions, analysis, and examples," *IEEE Trans. Power Syst.*, vol. 35, no. 1, pp. 13–29, 2020.

[29] D. K. Dheer, O. V. Kulkarni, S. Doolla, and A. K. Rathore, "Effect of reconfiguration and meshed networks on the small-signal stability margin of droop-based islanded microgrids," *IEEE Trans. on Industry Applications*, vol. 54, no. 3, pp. 2821–2833, 2018.
[30] J. He and Y. W. Li, "Analysis, design, and implementation of virtual impedance for power electronics interfaced distributed generation," *IEEE Trans. on Industry Applications*, vol. 47, no. 6, pp. 2525–2538, 2011.
[31] C. X. Rosero, M. Velasco, P. Mart´ı, A. Camacho, J. Miret, and M. Castilla, "Analysis of consensus-based islanded microgrids subject to unexpected electrical and communication partitions," *IEEE Trans. Smart Grid*, vol. 10, no. 5, pp. 5125–5135, 2019.
[32] ——, "Active power sharing and frequency regulation in droop-free control for islanded microgrids under electrical and communication failures," *IEEE Trans. Ind. Electron.*, vol. 67, no. 8, pp. 6461–6472, 2020.
[33] J. Zhang, M. Lyu, T. Shen, L. Liu, and Y. Bo, "Sliding mode control for a class of nonlinear multi-agent system with time delay and uncertainties," *IEEE Trans. Ind. Electron.*, vol. 65, no. 1, pp. 865–875, 2018.
[34] H. Markiewicz and A. Klajn, "Voltage disturbances standard en 50160 - voltage characteristics in public distribution systems," 2008.
[35] A. Levant, "Higher-order sliding modes, differentiation and output-feedback control," *International Journal of Control*, vol. 76, no. 9-10, pp. 924–941, 2003.
[36] W. Perruquetti and J. P. Barbot, *Sliding mode control in engineering*. CRC Press LLC, 2002.
[37] A. Shotorbani, B. Mohammadi-ivatloo, L. Wang, S. Ghassemzadeh, and S. H. Hosseini, "Distributed secondary control of battery energy storage systems in a stand-alone microgri," *IET Generation, Transmission Distribution*, vol. 12, 2018.

Carlos Alfaro was born in San Salvador, El Salvador. He received the B.S. in mechanical engineering from the Universidad Centroamericana "José Simeón Cañas" (UCA), El Salvador, in 2015, and M.S. in automatic systems and industrial electronics engineering from the Technical University of Catalonia, Spain, in 2018. He is currently working toward the Ph.D. degree in electronics at the Department of Electronic Engineering, Technical University of Catalonia. His current research interests include power electronics, nonlinear and predictive control.

Ramon Guzman received the B.S., the M.S. and the Ph.D. degrees in telecommunications engineering from the Technical University of Catalonia, Barcelona, Spain, in 1999, 2004 and 2016, respectively. He is currently an Associate Professor with the Department of Automatic Control in the Technical University of Catalonia. His research interests include nonlinear and adaptive control for three-phase power converters. Ramon Guzman is a member of the IEEE Industrial Electronics Society and becomes to the Renewable Energy Systems Subcommittee of Power Electronics Technical Committee of IES. Dr. Guzman is an Associate Editor of the IEEE Transactions on Industrial Electronics.

Luis Garcia de Vicuña received the Ingeniero de Telecomunicación and Dr.Ing. degrees in telecommunication engineering from the Technical University of Catalonia, Barcelona, Spain, in 1980 and 1990, respectively, and the Dr.Sci. degree from the Université Paul Sabatier, Toulouse, France, in 1992. He is currently a Full Professor in the Department of Electronic Engineering, Technical University of Catalonia, where he teaches courses on power electronics. His research interests include power electronics modeling, simulation and control, active power filtering, and high-power-factor ac/dc conversion.

Hasan Komurcugil (Senior Member, IEEE) received the B.Sc., M.Sc. and Ph.D. degrees from the Eastern Mediterranean University (EMU), Famagusta, North Cyprus, Via Mersin 10, Turkey, in 1989, 1991, and 1998, respectively, all in electrical engineering. He is currently full-time Professor with the Computer Engineering Department, EMU. From 2004 to 2010, he was the Head of the Computer Engineering Department, EMU. In 2010, he played an active role in preparing the department's first self-study report for the use of Accreditation Board for Engineering and Technology. In 2010, he was elected as the as the Board Member of Higher Education, Planning, Evaluation, Accreditation and Coordination Council (YODAK) North Cyprus. From 2010 to 2019, he played active role in evaluating the universities in North Cyprus. His research interests include power electronics and innovative control methods for power converters such as sliding mode control, Lyapunov-based control, and model predictive control. He is a coauthor of one book (Multilevel Inverters: Introduction and Emergent Topologies) chapter. He was the recipient of the best presentation recognitions at the 41st and 42nd annual conferences of the IEEE Industrial Electronics Society (IECON) in 2015 and 2016, respectively. He is a member of the IEEE Industrial Electronics Society (IES) and Senior Member of the IEEE. Also, he is the Chair of the Renewable Energy Systems Subcommitee of Power Electronics Technical Committee of IES. He served as the Corresponding Guest Associate Editor of the IEEE TRANSACTIONS ON ENERGY CONVERSION and Guest Editor of the IEEE TRANSACTIONS ON INDUSTRIAL INFORMATICS. Currently, he serves as the Associate Editor of the IEEE TRANSACTIONS ON INDUSTRIAL ELECTRONICS and the IEEE TRANSACTIONS ON INDUSTRIAL INFORMATICS.

Helena Mart´ın B.Sc. degree in Electronic Engineering, M.Sc. degree in Electrical Engineering, Ph.D. in Industrial Engineering, Polytechnic University of Catalonia (UPC). Her research interests are aligned with optimal sizing and management of microgrids, energy policies for the promotion of renewable generation and decarbonization and inverter control and grid synchronization techniques.